energies

MDPI

Article

Wavelet Scale Variance Analysis of Wind Extremes in Mountainous Terrains

Luciano Telesca [1,*], Fabian Guignard [2], Nora Helbig [3] and Mikhail Kanevski [2]

[1] Institute of Methodologies for Environmental Analysis, National Research Council, 85050 Tito (PZ), Italy
[2] IDYST, Faculty of Geosciences and Environment, University of Lausanne, CH-1015 Lausanne, Switzerland
[3] WSL Institute for Snow and Avalanche Research SLF, 7260 Davos, Switzerland
* Correspondence: luciano.telesca@imaa.cnr.it

Received: 12 June 2019; Accepted: 2 August 2019; Published: 7 August 2019

Abstract: The 10-min average wind speed series recorded at 130 stations distributed rather homogeneously in the territory of Switzerland are investigated. Fixing a percentile-based threshold of the wind speed distribution, a wind extreme is defined as the duration of the sequence of consecutive wind values above the threshold. This definition allows to analyze the sequence of extremes as a temporal point process marked by their duration. Representing the sequence of wind extremes by the inter-extreme interval series, the wavelet variance, a useful tool to investigate the variance of a time series across scales, was applied in order to find a link between the wavelet scales and several topographic parameters. Our findings suggest that the mean duration of wind extremes and mean inter-extreme time are positively correlated and that such relationship depends on the threshold of the wind speed. Furthermore, the threshold of the wind speed distribution correlates best with a terrain parameter related to the Laplacian of terrain elevations; and, in particular, for wavelet scales less than 3, the terrain exposure may explain the formation of extreme wind speeds.

Keywords: wind; extremes; wavelet

1. Introduction

Wind represents an important factor that not only studies the problems devoted to climate dynamics but also to energy generation [1], air pollution control [2], civil engineering [3], aeolian sediment transport [4], just to mention few of them. The fluctuations of wind speed that take place in the near-surface are typically characterized by irregularity and complexity, due to the interaction of several factors, like pressure gradient, turbulence phenomena, temperature, morpho-topographic conditions [5]. Models, like wind tunnel simulations [6] or computational fluid dynamics methods [7] that are traditionally used to perform simulations, were quite limited in disclosing the dynamical complexity of wind field. Thus, to characterize the dynamics of wind speed series, robust methods have been employed, like distributional analysis [8], chaotic time series analysis [9], wavelets [10], fractal and multifractal analysis [11–17], multiscale entropy analysis [18], multiscale multifractal analysis [19]. Most of the studies on wind speed were based on hourly or daily averages; however, to detect inner characteristics of the wind dynamics, like turbulence phenomena [20], and to understand complex dynamical patterns at very low timescales, high-frequency wind records are necessary.

Recently, the analysis of extremes in environmental data, including wind fields, attracted an important attention in renewable energy studies. Extremes are a natural part of the environmental phenomena but difficult to model and analyze. Study of the extremes is interesting both from fundamental scientific (stimulating developments of new methods and tools) and practical (power generation management, risk assessments, climate change influence on renewable energy potential estimation) points of view. An important issue, where the analysis of extremes can be useful as well,

is a selection of the relevant sites for the power stations. Taking into account the above-mentioned comments, a highly variable mountainous region like Switzerland can be a good example to study wind speed patterns, especially extremes.

Extremes are generally defined as values beyond a threshold that depends on the distribution and on how far into the tail of the distribution the threshold is located. Typically, values located in the far tail of the distribution are considered in societal and natural systems much more than those occurring more frequently because they are associated to a higher probability to cause large damage.

Extremes defined on the basis of percentiles of the distribution are frequently employed in climate studies because they could lead to a sufficiently large sample of data for robust statistical assessments [21]. In hydrology, for instance, Froidevaux et al. [22] showed that more than 20% of all flood events in Swiss catchments with a 5-year return period are preceded by 2-day precipitation sums between the 95th and the 99th percentile. Klawa and Ulbrich [23] investigated large-scale windstorms that affected large areas and produced large losses. Due to the particular morphological and topographic characteristics of each station, they proposed to normalize wind speed with a local extreme wind speed to filter out the effect of differences in wind climate and permit to spatially interpolate normalized station wind speeds. In their study, it was found that a 98th percentile of the wind speed distribution could allow to take sufficiently into account the possible damages produced by windstorms. Martius et al. [21] analyzed the co-occurrence of wind and rainfall extremes, both defined as the values above the 98th percentile of the corresponding distributions.

In this study, we investigate extremes of high-frequency wind speed time series in Switzerland using the wavelet variance analysis. We explored whether specific scales of the scale-dependent variance decomposition of the interevent time series of the extremes are linked to topographic characteristics with different grid resolutions ranging from fine- to coarse-scale.

The paper is organized as follows. Wind speed data and digital elevation model are introduced in Section 2. The wind extreme definition and the wavelet variance analysis are described in Section 3. Results and conclusion are drawn in the two last sections. Finally, in References, the main and the most relevant bibliographic references are listed.

2. Data

The wind speed series were measured by the MeteoSwiss weather network at 130 stations almost homogeneously distributed all over the territory of Switzerland from 2008 to 2017 (Figure 1 shows a map of Switzerland with the stations). The wind stations are located in roughly three climatic zones of Switzerland: Alps, Jura, and Plateau. The data were recorded with a sampling time of 10 min. Before being available on line for users, quality controls were carried out on the data by MeteoSwiss [24]. The missing values represent 2.4% of the data set. They were replaced by a 24-spatiotemporal neighbors local average, i.e., the mean of the eight closer stations in space and the two contiguous time frames [25,26].

All fine-scale terrain characteristics were obtained from a digital elevation model (DEM) produced by Swisstopo with a fine grid cell size $\Delta x = \Delta y = 25$ m. For the coarse-scale terrain characteristics, we averaged the 25 m DEM to $\Delta x = \Delta y = 250$ m and 1000 m, respectively, and derived the terrain characteristics at the corresponding resolutions. Subgrid terrain characteristics are derived from the DEM with $\Delta x = 25$ m and then spatially averaged to $\Delta x = 250$ m and 1000 m.

For each grid cell, we derived a parameter related to the Laplacian of terrain height z ($\nabla^2 z$), with regards to its immediate four neighbors. It is computed as $\nabla^2 z = \nabla^2 z' \Delta x/4$ with the discrete Laplacian $\nabla^2 z' = (z\,(x - \Delta x,y) + z\,(x + \Delta x,y) + z\,(x,y - \Delta x) + z\,(x,y + \Delta x) - 4z(x,y))/\Delta x^2$ and grid cell size $\Delta x = \Delta y$. If a surface is exposed compared to its surroundings, $\nabla^2 z$ is negative, and if a surface is sheltered, then, $\nabla^2 z$ is positive. A parameter related to the mean-squared slope (μ) is derived from first partial derivatives of the terrain height z for each grid cell:

$$\mu = \left\{ \left[\overline{(\partial_x z)^2 + \left(\partial_y z\right)^2} \right] \right\}^{1/2} \quad (1)$$

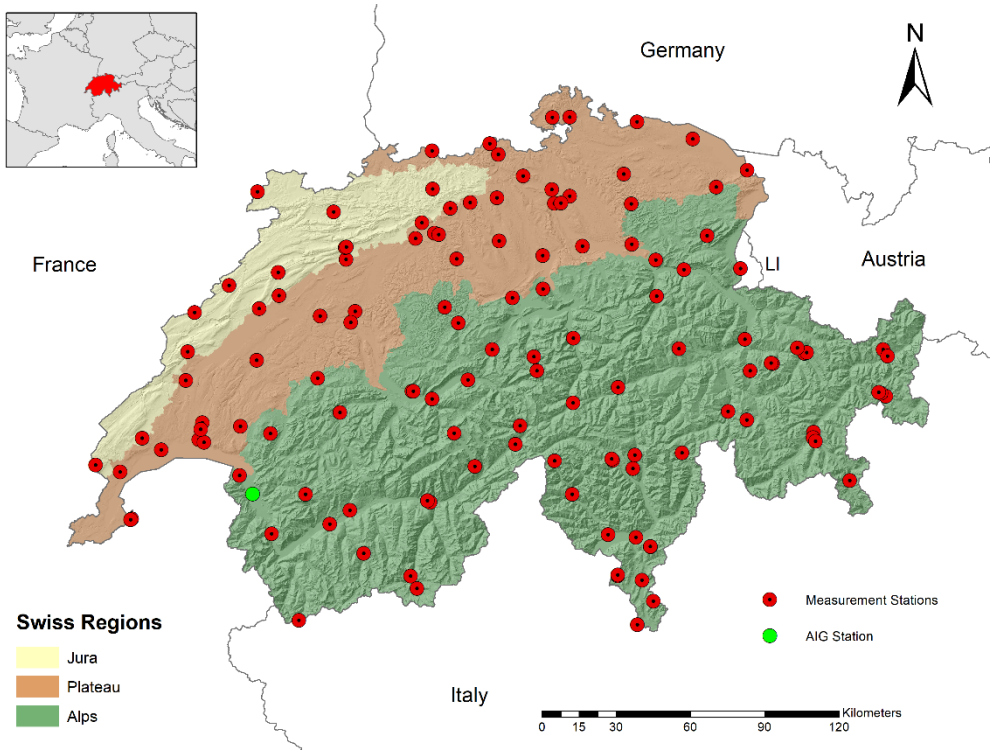

Figure 1. Map of Switzerland and location of the meteorological stations. AIG station is marked in green.

3. Methods

3.1. Definition of Wind Extremes and Their Statistical Features

Three thresholds were investigated—95th, 97.5th, and 99th percentiles of the wind speed distribution at each station. On the basis of the run theory [27], a "*run*" is defined as a sequence of contiguous values above a given percentile-based threshold. A *run* is characterized by its length, that is, the period m (or duration of the extreme) in which the variable under study is above the selected threshold. Hereafter, wind extreme is a *run* with a specific length m. This definition takes into account not only the wind speed that should be above a certain threshold but also its persistence in time since, supposedly, an extreme that lasts longer than another should very probably impact more intensively.

A sequence of *runs* or extremes can be viewed as a point process in time. Indicating with t_i the time at which the *run* starts or the extreme event occurs (hereafter, time of the *run*) and with m_i its length or duration of the extreme, the sequence of extremes can be described as a finite sum of Dirac's delta functions centered on the time t_i and amplitude proportional to m_i:

$$y(t) = \sum_{i=1}^{N} m_i \delta(t - t_i) \quad (2)$$

where N is the length of the sequence of extremes.

3.2. The Wavelet Variance

Multiresolution wavelet analysis makes possible a scale-dependent variance decomposition of a signal [28]. First, the time series $x = \{x_i\}$ is projected on a wavelet basis, yielding wavelet coefficients [29]. The wavelet basis is itself generated by translating and scaling a mother wavelet function noted $\psi(t)$. In practice, these coefficients are computed by a discrete wavelet transform [30].

Let's note S the maximal scale of the analysis. For each scale $s = 1, \ldots, S$ one has N_s wavelet coefficients available, given by

$$W_{s,n} = 2^{-\frac{s}{n}} \sum_{i=0}^{L-1} x_i \Psi(2^{-s}\mathrm{i} - \mathrm{n}) \tag{3}$$

for $n = 0, \ldots, N_s - 1$ and with L the length of the signal. If the length of the signal is a power of 2, then the number of coefficients per scale is $N_s = L/2^s$. Small scales correspond to high frequencies and large scales to low frequencies of the signal.

After that, the corresponding wavelet coefficients are used to obtain the wavelet variance for a given scale, and are defined as follows

$$\sigma^2_{wav}(s) = \frac{1}{2^s N_s} \sum_{n=0}^{N_s-1} \left[W_{s,n} - \sum_{n=0}^{N_s-1} W_{s,n} \right]^2 \tag{4}$$

which is an estimate of the variance of the wavelet coefficients at scale s divided by 2^s.

To see that, under some hypothesis, the wavelet variance is a scale decomposition of the signal variance. Let us suppose that the averages of the coefficient are zero. Then, the wavelet variance becomes

$$\sigma^2_{wav}(s) = \frac{1}{L} \sum_{n=0}^{N_s-1} W^2_{s,n} \tag{5}$$

for all scales s.

Assuming the orthonormality of the wavelet basis, one can show [28,31] that

$$\sum_{i=0}^{L-1} x_i^2 = \sum_{s=1}^{S} \sum_{n=0}^{N_s-1} W^2_{s,n} + L\,\bar{x}^2 \tag{6}$$

where $\bar{x}$ stands for the average of the signal.

Thus, using the two last equations, one arrives at the following relationship

$$\sum_{s=1}^{S} \sigma^2_{wav}(s) = \frac{1}{L} \sum_{s=1}^{S} \sum_{n=0}^{N_s-1} W^2_{s,n} = \frac{1}{L} \sum_{i=0}^{L-1} x_i^2 - \bar{x}^2 \tag{7}$$

i.e., the sum of the wavelet variance across the scales is equal to the sample variance of the original signal.

Therefore, the wavelet coefficients yield a natural decomposition of the signal variance by scale.

4. Results

Surface wind speed is considerably influenced by topography, leading to speed-up when a surface is exposed and to drag when a surface is sheltered relative to its surrounding topography. Often, horizon line related terrain parameters are used to describe this wind speed behavior in complex topography. Recently, among different tested terrain parameters, the best correlation between near-surface wind speed and fine-scale terrain parameters was found for the parameter related to the Laplacian of terrain elevations [32]. Indeed, a similar non-dimensional version of the Laplacian on resolved terrain elevations was used by Jimenez and Dudhia [33] to describe unresolved terrain exposure and sheltering of simulated coarse-scale surface wind speed.

Naturally, in the complex topography, the degree of immediate exposure of a surface contributes to the formation of extreme wind speed. Therefore, we investigated correlations of the three percentile thresholds of the measured wind speed distribution used to characterize extreme wind speed events with various terrain parameters. Though terrain elevation was also significantly correlated with the three percentile thresholds of wind speed for some scales, we again obtained the best correlation with the parameter related to the Laplacian of terrain elevations $\nabla^2 z$. For all three percentile thresholds and the corresponding measured wind speed values, we obtained significant Spearman correlation coefficients about 0.3 with $\nabla^2 z$ derived on a DEM with horizontal grid cell resolution of 25 m. Because of the definition of $\nabla^2 z$, the correlation is negative with increasing wind speed.

Figure 2a shows, as an example, the sequence of wind extremes (for the threshold of 95th percentile of the distribution of the wind speed) for the station AIG at 381 m a.s.l., where the duration m is indicated by amplitude of each extreme. The sequence of wind extremes can be represented by the inter-extreme times $T_k = t_{k+1} - t_k$, where t_k indicates the time of the extreme numbered by the index k. Figure 2b shows the inter-extreme time series of the wind extremes shown in Figure 2a.

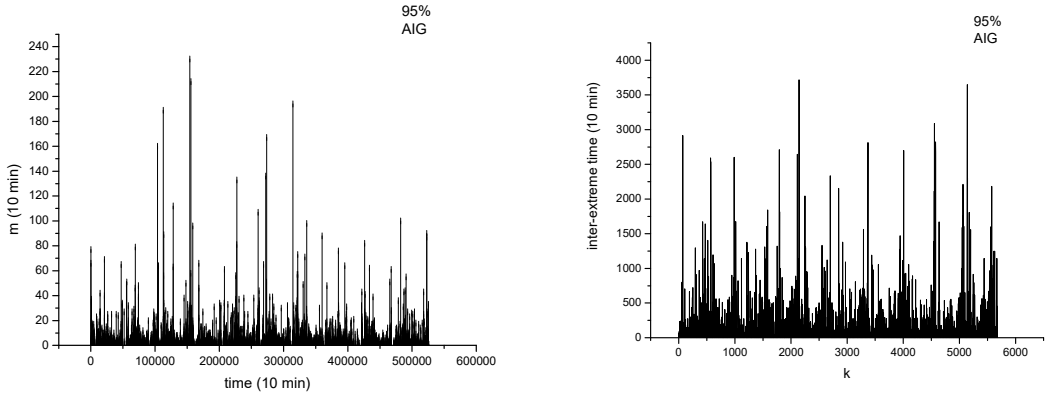

(**a**) (**b**)

Figure 2. Sequence of wind extremes (for the threshold of 95th percentile of the distribution of the wind speed) for the station AIG at 381 m a.s.l.: (**a**) durations m and (**b**) inter-extreme times.

Investigating the link between the mean inter-extreme time and the mean duration <m> of wind extremes, a clear linear relationship was found for all the three thresholds (Figure 3). This suggests that the longer the duration of the extremes, the larger the time between two successive extremes. Furthermore, the mean inter-extreme time increases with the increase of the threshold, i.e., the rarer the extreme wind events, the larger the time in-between such an event.

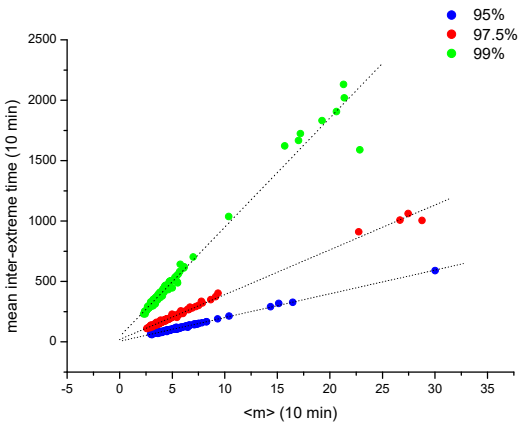

Figure 3. Relationship between the mean inter-extreme time and the mean duration <m> of wind extremes.

The relationship between the mean duration and the mean inter-extreme time of wind extremes with the main morpho-topographic features of the Swiss territory seems to be dependent only on the threshold; Figure 4 shows, as an example, <*m*> (Figure 4a) and the mean inter-extreme time (Figure 4b) versus altitude.

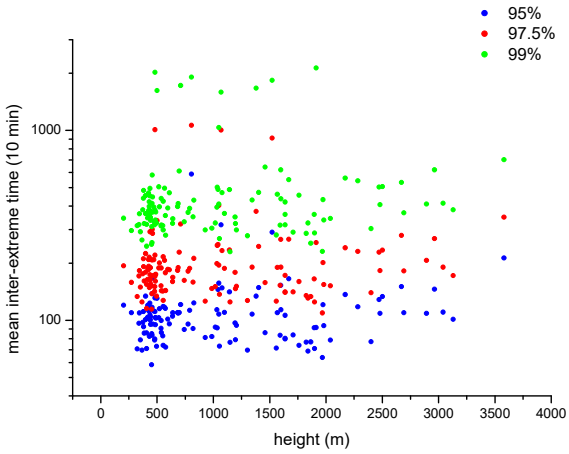

(**a**)

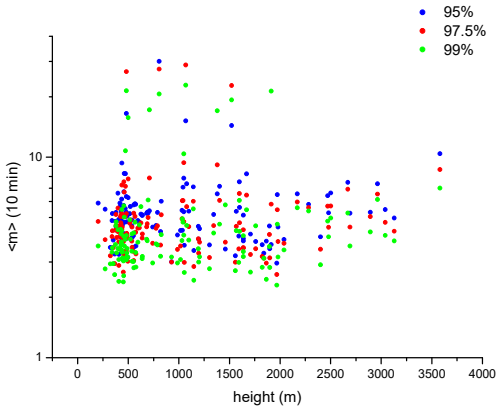

(**b**)

Figure 4. Relationship of (**a**) mean inter-extreme time and (**b**) mean duration with height across the stations.

For each threshold we calculated the wavelet variance of the inter-extreme times of the wind extremes at each station by using the mother wavelet db10. Figure 5 shows, as an example, the 3-D plot of the wavelet coefficients for the station AIG (95th percentile threshold), while Figure 6 shows the wavelet variance of the coefficients shown in Figure 5.

For each site characterized by the morpho-topographic features, hereafter generically indicated as v, we calculated the wavelet variance $\sigma_w(s)$ of the inter-extreme time series; s represents the wavelet scale. Thus, fixing the scale s, we calculated the Spearman rank correlation coefficient and its p-value between the $\sigma_w{}^2(s)$ and v. Table 1 shows the correlation between the wavelet variance and the height. Considering the significance level of 0.01 for the p-value, such correlation is not significant for 95% threshold; it is significant only at scale 6 for 97.5% threshold and at lower scales, from 1 to 3, for 99%. This could suggest that there are specific scales that are more sensitive to the influence of a particular topographic parameter.

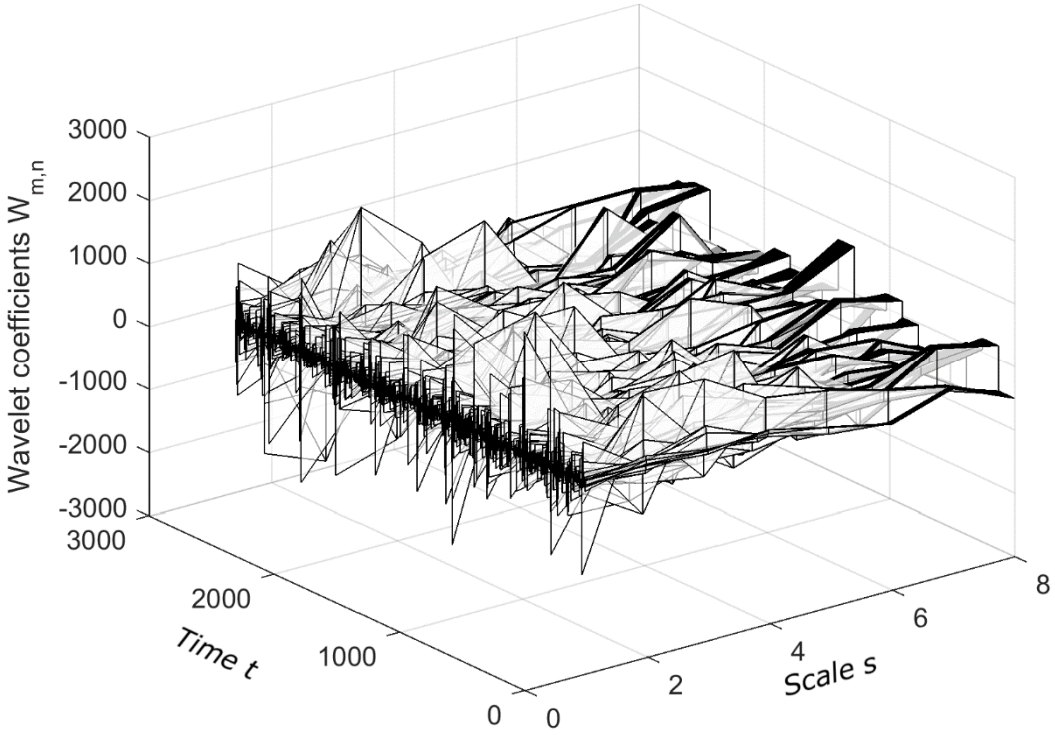

Figure 5. 3-D plot of the wavelet coefficients for station AIG (95th percentile threshold).

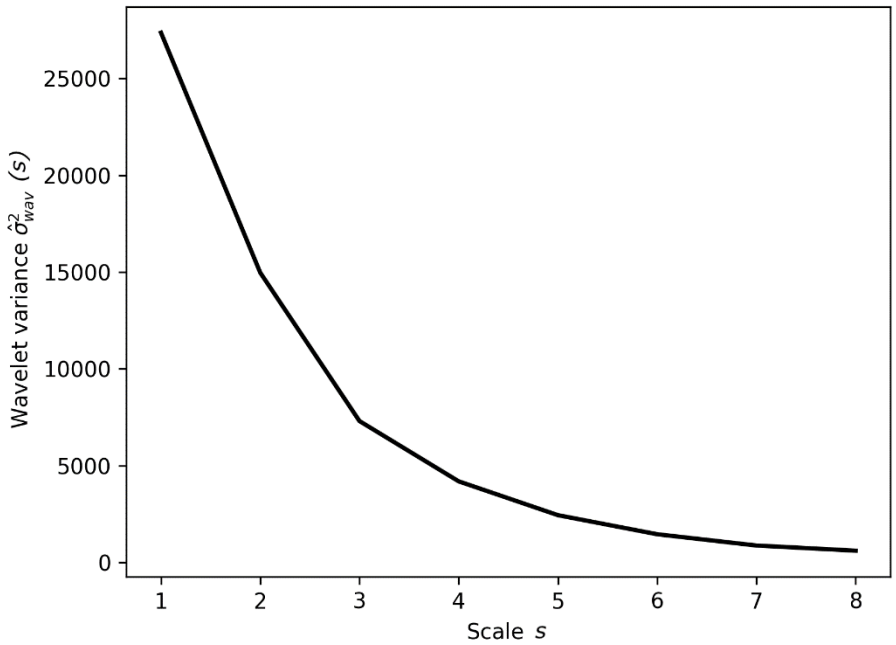

Figure 6. Wavelet variance of the coefficients shown in Figure 5.

At scales s from one to three, the most statistically significant behavior for all threshold percentiles was found almost consistently for two topographic parameters, namely $\nabla^2 z$ and μ (Tables 2 and 3). Among all spatial scales, subgrid (sbg) μ derived for Δx of 250 m shows the most dominant influence on the wavelet variance of the inter-extreme times for μ. The Spearman r is between 0.25 and 0.3 for the 99% percentile threshold and scale s of one (Table 2). Regarding $\nabla^2 z$, the greatest influence among all spatial scales was achieved with $\nabla^2 z$ derived on Δx of 1000 m for the 97.5% percentile threshold and scale s of three, with a Spearman r of 0.32 (Table 3).

Table 1. Spearman rank correlation r and its p-value between height and the wavelet variance of the inter-extreme time series of the wind extremes for different thresholds. The results below the significance level of 0.01 are in bold.

		95% Threshold		97.5% Threshold		99% Threshold	
	Scale	***r***	***p*-Value**	***r***	***p*-Value**	***r***	***p*-Value**
Δx = 25 m	1	0.19	0.039	0.19	0.033	0.27	**0.002**
	2	0.19	0.032	0.21	0.019	0.24	**0.007**
	3	0.17	0.059	0.19	0.034	0.26	**0.003**
	4	0.17	0.067	0.17	0.061	0.21	0.018
	5	0.15	0.109	0.21	0.016	0.17	0.059
	6	0.22	0.015	0.24	**0.006**	−0.13	0.138
	7	0.23	0.011	−0.13	0.147	-	-
	8	0.00	0.999	-	-	-	-

Table 2. Spearman rank correlation r and its p-value between the slope-related parameter μ and the wavelet variance of the inter-extreme time series of the wind extremes for different thresholds. The results below the significance level of 0.01 are in bold.

		95% Threshold		97.5% Threshold		99% Threshold	
	Scale	***r***	***p*-Value**	***r***	***p*-Value**	***r***	***p*-Value**
Δx = 25 m	1	0.19	0.034	0.20	0.026	0.25	**0.004**
	2	0.21	0.018	0.22	0.011	0.24	**0.006**
	3	0.21	0.018	0.22	0.011	0.23	**0.009**
sbg 250 m	1	0.25	**0.005**	0.25	**0.004**	0.30	**0.001**
	2	0.26	**0.003**	0.28	**0.001**	0.28	**0.001**
	3	0.25	**0.004**	0.26	**0.003**	0.28	**0.001**
sbg 1000 m	1	0.23	**0.008**	0.22	0.011	0.28	**0.001**
	2	0.23	**0.007**	0.24	**0.006**	0.24	**0.006**
	3	0.21	0.016	0.23	**0.009**	0.26	**0.003**

Table 3. Spearman rank correlation r and its p-value parameter $\nabla^2 z$ related to the Laplacian of terrain height z and the wavelet variance of the inter-extreme time series of the wind extremes for different thresholds. The results below the significance level of 0.01 are in bold.

		95% Threshold		97.5% Threshold		99% Threshold	
	Scale	***r***	***p*-Value**	***r***	***p*-Value**	***r***	***p*-Value**
Δx = 25 m	1	0.18	0.037	0.17	0.055	0.15	0.089
	2	0.20	0.022	0.18	0.043	0.15	0.082
	3	0.22	0.012	0.20	0.023	0.11	0.206
Δx = 250 m	1	0.16	0.062	0.16	0.075	0.17	0.054
	2	0.15	0.083	0.14	0.118	0.18	0.035
	3	0.15	0.081	0.17	0.056	0.21	0.019
Δx = 1000 m	1	0.27	**0.002**	0.31	**0.000**	0.28	**0.001**
	2	0.27	**0.002**	0.27	**0.002**	0.30	**0.001**
	3	0.28	**0.001**	0.32	**0.000**	0.28	**0.001**

While for both topographic parameters at larger scales s even better correlations were sometimes observed, at these scales there is less grouping among each percentile thresholds (not shown).

5. Conclusions

In this study, the sequences of extremes in wind speed measured by 130 stations of the MeteoSwiss weather network in Switzerland were analyzed by using the wavelet variance. The main findings

can be summarized as follows: (i) a clear relationship exists between mean duration of extremes and mean inter-extreme times so that the longer the duration of the extremes, the larger the time between two successive extremes; (ii) the mean inter-extreme time increases with the increase of the threshold of the wind speed; (iii) the relationship between the mean duration of wind extremes and the mean inter-extreme time depends on the threshold of wind speed; (iv) the three percentile-based thresholds of the measured wind speed distribution correlates best with a terrain parameter related to the Laplacian of terrain elevations $\nabla^2 z$ which is in agreement with previous findings for near-surface wind speed [32]; (v) the correlation between the wavelet variance $\sigma_w(s)$ of the inter–extreme time series and terrain parameters changes with the scale s, the threshold percentiles of the wind speed distribution, and the horizontal grid cell size the terrain parameter were derived for. Thus, $\sigma_w(s)$ provides some guidance for identifying scales s where the effect of a particular topographic parameter is more dominant. For $s \leq 3$ the best correlations were consistently obtained for all percentile thresholds for $\nabla^2 z$ computed on a DEM with Δx of 1000 m. Similar good correlations were consistently obtained for all percentile thresholds for $s \leq 3$ for subgrid (sbg) μ derived for Δx of 250 m and 1000 m. For $s \leq 3$ terrain elevation z only showed significant (p-value < 0.01) correlations for a percentile threshold of 99%. In conclusion, this suggests that at these scales s terrain exposure may indeed explain the formation of extreme wind speeds.

In conclusion, the fundamental research carried out can be practically used for aeolian energy issues: Estimation of wind energy potential assessment and production management taking into account extreme events temporal variability at different scales and their relationship to complex topography.

Author Contributions: Software: L.T. and F.G.; formal analysis: L.T., F.G., N.H.; investigation: L.T., N.H. and M.K.; writing, original draft preparation, L.T.; writing, review and editing, L.T., F.G., N.H., M.K.; visualization, F.G. and N.H.; supervision, M.K.; project administration, M.K.; funding acquisition, L.T., F.G. and M.K.

Funding: This research was funded by SNSF "Scientific Exchanges" project n° 180296 (L.T.) and by National Research Programme "Big Data" (PNR75) of the Swiss National Science Foundation (SNSF), project "Hybrid Renewable Energy Potential for the Built Environment using Big Data: Forecasting and Uncertainty Estimation" (N 4075-40_167285) (F.G. and M.K.)

Conflicts of Interest: The authors declare no conflict of interest.

References

1. Ummels, B.C.; Gibescu, M.; Pelgrum, E.; Kling, W.L.; Brand, A.J. Impacts of Wind Power on Thermal Generation Unit Commitment and Dispatch. *IEEE Trans. Energy Convers.* **2007**, *22*, 44–51. [CrossRef]
2. Demirci, E.; Cuhadaroglu, B. Statistical analysis of wind circulation and air pollution in urban Trabzon. *Energy Build.* **2000**, *31*, 49–53. [CrossRef]
3. Cermak, J.E. Wind-tunnel development and trends in applications to civil engineering. *J. Wind Eng. Ind. Aerodyn.* **2003**, *91*, 355–370. [CrossRef]
4. Sterk, G.; Jacobs, A.F.G.; Van Boxel, J.H. The effect of turbulent flow structures on saltation sand transport in the atmospheric boundary layer. *Earth Surf. Proc. Land.* **1998**, *23*, 877–887. [CrossRef]
5. Kavasseri, R.G.; Nagarajan, R. Evidence of crossover phenomena in wind-speed data. *IEEE Trans Circuits Syst. I* **2004**, *51*, 2255–2262. [CrossRef]
6. Raupach, M.R.; Thom, A.S.; Edwards, I. A wind-tunnel study of turbulent flow close to regularly arrayed rough surfaces. *Bound. Layer Meteorol.* **1980**, *18*, 373–397. [CrossRef]
7. Parsons, D.R.; Walker, I.J.; Wiggs, G.F.S. Numerical modelling of flow structures over idealized transverse aeolian dunes of varying geometry. *Geomorphology* **2004**, *59*, 149–164. [CrossRef]
8. Celik, A.N. A statistical analysis of wind power density based on the Weibull and Rayleigh models at the southern region of Turkey, April 2004. *Renew. Energy* **2004**, *29*, 593–604. [CrossRef]
9. Karakasidis, T.E.; Charakopoulos, A. Detection of low-dimensional chaos in wind time series. *Chaos Solit. Fractals* **2009**, *41*, 1723–1732. [CrossRef]
10. Avdakovic, S.; Lukac, A.; Nuhanovic, A.; Music, M. Wind Speed Data Analysis using Wavelet Transform. *Int. J. Environ. Chem. Ecol. Geol. Geophys. Eng.* **2011**, *5*, 138–142.

11. Kavasseri, R.G.; Nagarajan, R. A multifractal description of wind speed records. *Chaos Solit. Fractals* **2005**, *24*, 165–173. [CrossRef]
12. Kavasseri, R.G.; Nagarajan, R. A qualitative description of boundary layer wind speed records. *Fluct. Noise Lett.* **2006**, *6*, 201–213. [CrossRef]
13. Koçak, K. Examination of persistence properties of wind speed records using detrended fluctuation analysis. *Energy* **2009**, *34*, 1980–1985. [CrossRef]
14. Santos, M.D.O.; Stosic, T.; Stosic, B.D. Long-term correlations in hourly wind speed records in Pernambuco. *Braz. Phys. A* **2012**, *391*, 1546–1552. [CrossRef]
15. Feng, T.; Fu, Z.T.; Deng, X.; Mao, J.Y. A brief description to different multi-fractal behaviors of daily wind speed records over China. *Phys. Lett. A* **2009**, *373*, 4134–4141. [CrossRef]
16. Telesca, L.; Lovallo, M. Analysis of the time dynamics in wind records by means of multifractal detrended fluctuation analysis and the Fisher—Shannon information plane. *J. Stat. Mech.* **2011**, *2001*, P07001. [CrossRef]
17. Telesca, L.; Lovallo, M.; Kanevski, M. Power spectrum and multifractal detrended fluctuation analysis of high-frequency wind measurements in mountainous regions. *Appl. Energy* **2016**, *162*, 1052–1061. [CrossRef]
18. Fu, Z.T.; Li, Q.L.; Yuan, N.M.; Yao, Z.H. Multi-scale entropy analysis of vertical wind variation series in atmospheric boundary-layer. *Commun. Nonlinear Sci. Numer. Simul.* **2014**, *19*, 83–91. [CrossRef]
19. Zeng, M.; Zhang, X.-N.; Li, J.-H.; Meng, Q.-H. The Scaling Properties of High-frequency Wind Speed Records Based on Multiscale Multifractal Analysis. *Acta Phys. Pol. B* **2016**, *47*, 2205–2224. [CrossRef]
20. Walker, I.J. Physical and logistical considerations of using ultrasonic anemometers in aeolian sediment transport research. *Geomorphology* **2005**, *68*, 57–76. [CrossRef]
21. Martius, O.; Pfahl, S.; Chevalier, C. A global quantification of compound precipitation and wind extremes. *Geophys. Res. Lett.* **2016**, *43*, 7709–7717. [CrossRef]
22. Froidevaux, P.; Schwanbeck, J.; Weingartner, R.; Chevalier, C.; Martius, O. Flood triggering in Switzerland: The role of daily to monthly preceding precipitation. *Hydrol. Earth Syst. Sci.* **2015**, *19*, 3903–3924. [CrossRef]
23. Klawa, M.; Ulbrich, U. A model for the estimation of storm losses and the identification of severe winter storms in Germany. *Nat. Hazards Earth Syst. Sci.* **2003**, *3*, 725–732. [CrossRef]
24. MeteoSwiss. Automatic Monitoring Network, Internal Report. 2018. Available online: https://www.meteoswiss.admin.ch (accessed on 5 August 2019).
25. Jun, M.; Stein, M.L. An approach to producing space: Time covariance functions on spheres. *Technometrics* **2007**, *49*, 468–479. [CrossRef]
26. Porcu, E.; Bevilacqua, M.; Genton, M.G. Spatio-temporal covariance and cross-covariance functions of the great circle distance on a sphere. *J. Am. Stat. Assoc.* **2016**, *111*, 888–898. [CrossRef]
27. Cramer, H.; Leadbetter, M.R. *Stationary and Related Stochastic Processes*; Dover Publications Inc.: Mineaola, NY, USA, 1967.
28. Lindsay, R.W.; Percival, D.B.; Rothrock, D.A. The discrete wavelet transform and the scale analysis of the surface properties of sea ice. *IEEE Trans. Geosci. Rem. Sens.* **1996**, *34*, 771–787. [CrossRef]
29. Thurner, S.; Feurstein, M.; Teich, M.C. Multiresolution wavelet analysis of heartbeat intervals discriminates healthy patients from those with cardiac pathology. *Phys. Rev. Lett.* **1997**, *80*, 1544–1547. [CrossRef]
30. Daubechies, I. *Ten Lectures on Wavelets*; Society for Industrial and Applied Mathematics: Philadelphia, PA, USA, 1992.
31. Addison, P.S. *The Illustrated Wavelet Transform Handbook*; Taylor & Francis: Didcot/Abingdon, UK, 2002.
32. Helbig, N.; Mott, R.; van Herwijnen, A.; Winstral, A.; Jonas, T. Parameterizing surface wind speed over complex topography. *J. Geophys. Res. Atmos.* **2017**, *122*, 651–667. [CrossRef]
33. Jimenez, P.A.; Dudhia, J. Improving the representation of resolved and unresolved topographic effects on surface wind in the WRF model. *J. Appl. Meteorol. Climatol.* **2012**, *51*, 300–316. [CrossRef]